MODIFICATION OF THE STANDARD ϵ-EQUATION FOR THE STABLE ABL THROUGH ENFORCED CONSISTENCY WITH MONIN–OBUKHOV SIMILARITY THEORY

FRANK R. FREEDMAN and MARK Z. JACOBSON
Environmental Fluid Mechanics Laboratory, Department of Civil and Environmental Engineering, Stanford University, Stanford, CA 94305-4020, U.S.A.

(Received in final form 16 April 2002)

Abstract. A condition is derived for consistency of the standard ϵ-equation with Monin–Obukhov (MO) similarity theory of the stably-stratified surface layer. The condition is derived by extending the procedure used to derive the analogous condition for neutral theory to stable stratification. It is shown that consistency with MO theory requires a function of flux Richardson number, Ri_f, to be absorbed into either of two closure parameters, $c_{\epsilon 1}$ or $c_{\epsilon 2}$. Inconsistency, on the other hand, results if constant values of these are maintained for all Ri_f, as is done in standard application of the equation, and the large overpredictions of turbulence found in such application to the one-dimensional stable atmospheric boundary layer (1D-SBL) are traced to this inconsistency. Guided by this, we formulate a MO-consistent ϵ-equation by absorbing the aforementioned function into $c_{\epsilon 1}$, and combine this with a Level-2.5 second-order closure model for vertical eddy viscosity and diffusivities. Numerical predictions of the 1D-SBL by the modified model converge to a quasi-steady state, rectifying the predictive failure of the standard ϵ-equation for the case. Quasi-steady predictions of non-dimensional variables agree strongly with Nieuwstadt's theory. Qualitative accuracy of predictions is inferred from comparisons to field data, large-eddy simulation results and Rossby-number similarity relationships.

Keywords: ϵ-Equation, Level-2.5 model, Stable boundary layer, Turbulence parameterization.

1. Introduction

In modelling turbulence in stably-stratified conditions, the eddy viscosity, K_m, and heat diffusivity, K_h, must be decreased with increasing stability to account for buoyant suppression of vertical turbulent motion. The suppression of turbulent vertical velocity, w, is represented in second-order closure (SOC) models by explicitly appearing buoyancy destruction terms in the Reynolds stress and heat flux transport equations. In the Level-2.5 SOC model (Mellor and Yamada, 1982; hereafter MY82), elimination of growth rate and transport terms in these equations and use of the "boundary layer" assumption as well as others lead to $K_m = S_M l q$ and $K_h = S_H l q$. Here, q^2 is twice the turbulent kinetic energy (TKE), l is an independently modelled turbulent length scale, and S_M and S_H are 'stability functions', derived from algebraic forms of the SOC equations resulting from the above eliminations and assumptions. Most of the suppression of w by the buoyancy

Boundary-Layer Meteorology **106:** 383–410, 2003.

terms in the original SOC equations becomes in this model absorbed into S_M and S_H through their decreasing functionalities with respect to gradient Richardson number. The remainder is in the buoyancy term in the TKE equation.

Whereas the suppression of w is represented explicitly in the Level-2.5 model, the decision and manner to suppress l are at the discretion of the modeller. In addition to leaving l unchanged from traditional neutral algebraic forms, modellers have made various modifications to algebraic formulations for stable conditions, generally achieved by extending surface-layer profiles into the body of the ABL with limits proportional to local stability scales (e.g., Brost and Wyngaard, 1978; Lacser and Arya, 1986; Delage, 1997). Difficulties in formulating an algebraic l expression suitable for arbitrary geometries and/or turbulence state, however, have led to more wide use in engineering flow computation of a transport equation for a chosen scale quantity, of which the TKE dissipation rate, ϵ, is the most common. Because of the intractability of term-by-term closure of the exact transport equation for ϵ (Tennekes and Lumley, 1972), a standard modelled equation (referred to as the 'ϵ-equation') constructed by direct analogy to the TKE equation is employed for this purpose. Unreasonably large K_m and K_h, however, are predicted when the ϵ-equation is applied to the one-dimensional, horizontally homogeneous, stable atmospheric boundary layer (1D-SBL) (Wyngaard, 1975; Duynkerke, 1988; Andrén, 1991; Apsley and Castro, 1997). Because of this and other predictive errors in the neutral and unstably stratified horizontally homogeneous ABL (see Freedman and Jacobson (2002) for rectification of the former and Andrén (1991) for demonstration of the latter), the ϵ-equation has not seen wide use in meteorological flow computation in spite of its potential advantages in predicting ABLs whose structure diverges from classical 1D prototypes.

In this paper, we investigate the cause for the ϵ-equation's turbulence overpredictions of the 1D-SBL by deriving a condition for consistency of the equation with Monin–Obukhov (MO) similarity theory of the stably-stratified surface layer. MO theory is an extension of classical neutral surface-layer theory to account for stratification. Our consistency condition is thus the appropriate extension of that previously derived for consistency with neutral theory. In the neutral case, consistency is enforced by using the previously derived condition to set the value of the equation closure parameter σ_ϵ. In the stable case, our generalized condition instead yields a *function* of flux Richardson number, Ri_f, that must be absorbed into either of two closure parameters, $c_{\epsilon 1}$ or $c_{\epsilon 2}$, to enforce consistency. Inconsistency otherwise results if constant values for these are maintained for all Ri_f, as is done in standard application, and the aforementioned turbulence overpredictions of the 1D-SBL are traced to this inconsistency. Guided by this, we develop a MO-consistent ϵ-equation by absorbing the aforementioned function into $c_{\epsilon 1}$, and combine this with the Level-2.5 formulation of Andrén (1990) to yield a modified model for K_m and K_h. The model is evaluated by checking for convergence of its numerical 1D-SBL predictions to a quasi-steady state, not achieved with the standard form of the ϵ-equation. Additional predictive behaviour as well as accuracy is diagnosed

through comparing predictions with a variety of theoretical, observational and large-eddy simulation (LES) results.

2. Background

2.1. Basic equations

The 1D-SBL is governed by the following equations for mean horizontal streamwise (in the direction of the geostrophic wind) and cross-stream (perpendicular and to the left of the geostrophic wind) velocity components, U and V, respectively, and potential temperature, Θ,

$$\frac{\partial U}{\partial t} = fV - \frac{\partial \overline{uw}}{\partial z} \tag{1}$$

$$\frac{\partial V}{\partial t} = -f(U - G) - \frac{\partial \overline{vw}}{\partial z} \tag{2}$$

$$\frac{\partial \Theta}{\partial t} = -\frac{\partial \overline{w\theta}}{\partial z}. \tag{3}$$

Here, G is the geostrophic wind speed (taken independent of height), f is the Coriolis parameter, $\overline{uw}$ and $\overline{vw}$ are the u and v components of the vertical turbulent momentum flux (Reynolds stress), respectively, $\overline{w\theta}$ is the vertical turbulent heat flux, t is time and z is height. Diabatic sources and sinks are neglected in (3).

Fluxes are represented by gradient-diffusion expressions,

$$-\overline{uw} = c_m \frac{E^2}{\epsilon} \frac{\partial U}{\partial z} \tag{4}$$

$$-\overline{vw} = c_m \frac{E^2}{\epsilon} \frac{\partial V}{\partial z} \tag{5}$$

$$-\overline{w\theta} = c_h \frac{E^2}{\epsilon} \frac{\partial \Theta}{\partial z}. \tag{6}$$

From these, expressions for eddy viscosity, $K_m = c_m E^2/\epsilon$, and heat diffusivity, $K_h = c_h E^2/\epsilon$, are apparent. The turbulence Prandtl number, $Pr_t \equiv K_m/K_h = c_m/c_h$, follows from these. Here, E is the turbulent kinetic energy (TKE), ϵ the TKE dissipation rate, and c_m and c_h are stability functions. The above expressions for K_m and K_h can be cast in the form given in Section 1 by defining $l \propto E^{3/2}/\epsilon$ and associating $S_M \propto c_m$ and $S_H \propto c_h$.

The equation for E maintains its prognostic form,

$$\frac{\partial E}{\partial t} - \frac{\partial}{\partial z}\left(\frac{K_m}{\sigma_E}\frac{\partial E}{\partial z}\right) = P + B - \epsilon = P(1 - \mathrm{Ri}_f) - \epsilon, \tag{7}$$

where P and B,

$$P = -\overline{uw}\frac{\partial U}{\partial z} - \overline{vw}\frac{\partial V}{\partial z} \tag{8}$$

$$B = \frac{g}{\Theta_a}\overline{w\theta}, \tag{9}$$

are TKE shear and buoyancy production rates, respectively, σ_E is a closure parameter, g is the gravitational acceleration and Θ_a a background value of Θ. Equation (7) is written in terms of the flux Richardson number, $\mathrm{Ri}_f \equiv -B/P$, on the far right side. The *local equilibrium* assumption

$$P + B = P(1 - \mathrm{Ri}_f) = \epsilon \tag{10}$$

results from conditions where the local source and sink terms in (7) dominate.

For c_m and c_h, we use the Level-2.5 formulation of Andrén (1990), based on the 'full' (prior to elimination of terms in the second-moment transport equations) SOC of Gibson and Launder (1978, hereafter GL78). For simplicity, we neglect the parameterization of wall-proximity effects utilized by GL78 and Andrén (1990). The GL78 SOC differs from that used by MY82 in that additional terms are used in the former to represent the rapid part of pressure redistribution. Predictive advantages of the GL78 over MY82 SOC are shown in Speziale and MacGiolla-Mhuiris (1989); additional comments supporting the former are made by Andrén (1990).

The equations for c_m and c_h are given in Appendix A by (A1) and (A2), along with their local equilibrium forms, $c_{m,LE}$ and $c_{h,LE}$, by (A6) and (A7). It is seen that the latter two are a function only of gradient Richardson number, $\mathrm{Ri} \equiv -[g/\Theta_a \partial\Theta/\partial z]/[(\partial U/\partial z)^2 + (\partial V/\partial z)^2]$, and are thus determined solely from the mean variables. The local equilibrium form of flux Richardson number, $\mathrm{Ri}_{f,LE}$, is given by (A8), and is also only a function of Ri.

The model is closed by the standard ϵ-equation,

$$\frac{\partial \epsilon}{\partial t} - \frac{\partial}{\partial z}\left(\frac{K_m}{\sigma_\epsilon}\frac{\partial \epsilon}{\partial z}\right) = c_{\epsilon 1}\frac{\epsilon(P + B)}{E} - c_{\epsilon 2}\frac{\epsilon^2}{E}, \tag{11}$$

whose form is a dimensionally consistent analogy to (7). Rationale and additional ideas behind this are given in Launder (1989), Speziale and Bernard (1992), Speziale and Gatski (1996) and Wilcox (1998). Closure parameters $c_{\epsilon 1}$, $c_{\epsilon 2}$ and σ_ϵ are generally taken as constant values empirically determined to match laboratory flow data. The 'standard' values $c_{\epsilon 1} = 1.44$ and $c_{\epsilon 2} = 1.92$ in particular

were set to match data for neutrally-stratified unbounded turbulent flows (Durbin and Pettersson-Reif, 2001). It is shown below, however, that assigning constant values for both leads to an inconsistency with MO theory. The calibration of σ_ϵ is discussed in the next subsection. Finally, some modellers separate the shear and buoyancy contributions in (11) by introducing an additional closure parameter, $c_{\epsilon 3}$, multiplying the buoyancy term. For reasons discussed later, we choose not to make this separation.

2.2. Consistency condition – neutral case

The value of σ_ϵ is set by enforcing consistency of (11) with classical theory for a steady, neutrally-stratified surface layer (see Garratt, 1992, for a summary of the theory). The layer is characterized by constant shear stress and a logarithmic, unidirectional mean velocity profile, and hence

$$-\overline{uw} = u_\star^2 \tag{12}$$

$$\frac{\mathrm{d}U}{\mathrm{d}z} = \frac{u_\star}{kz}, \tag{13}$$

where $u_\star$ is the surface friction velocity and $k \approx 0.4$. Dividing (12) by (13) gives

$$K_m = u_\star kz. \tag{14}$$

In (12) and (13), the coordinate system is rotated so that u is along the surface shear stress. Since the flow is unidirectional, V and $\overline{vw}$ are thus zero in this coordinate system.

Since the surface layer is assumed in local equilibrium, consistency with neutral theory requires that the model's local equilibrium form is matched to (12)–(14). Inserting (12) and (13) into (8) and equating to ϵ gives

$$\epsilon = u_\star^3/kz. \tag{15}$$

Substituting (12), (13) and (15) into (4) then yields

$$E = c_{m,0}^{-1/2} u_\star^2, \tag{16}$$

where $c_{m,0}$, defined in (A6), is the value of c_m for neutral, local equilibrium conditions. Inserting (12)–(16) into the steady, neutral form of (11) then leads to

$$c_{\epsilon 2} - c_{\epsilon 1} = \frac{k^2 c_{m,0}^{-1/2}}{\sigma_\epsilon}. \tag{17}$$

Consistency with neutral theory is enforced by solving (17) for σ_ϵ with *a priori* determined values of k, $c_{\epsilon 1}$, $c_{\epsilon 2}$ and $c_{m,0}$. Taking the values above for the first three and the standard engineering value $c_{m,0} = 0.09$ gives $\sigma_\epsilon = 1.1$.

2.3. MONIN–OBUKHOV SIMILARITY THEORY

The following discusses elements of MO similarity theory (see Garratt (1992) for further details) needed for deriving an expression analogous to (17) for stable conditions. The flow architecture is as the neutral case but with a height-invariant surface heat flux $(\overline{w\theta})_0 < 0$ and associated stable stratification $d\Theta/dz > 0$. Dimensional arguments then suggest the following stability modification to (13),

$$\frac{\mathrm{d}U}{\mathrm{d}z} = \frac{u_\star}{kz}\phi_m(\xi), \tag{18}$$

where $\xi \equiv z/L$ is defined in terms of the Obukhov length,

$$L \equiv -\frac{u_\star^3 \Theta_a}{kg(\overline{w\theta})_0}. \tag{19}$$

Dividing (12) by (18) gives

$$K_m = u_\star kz/\phi_m. \tag{20}$$

Scaling arguments then suggest

$$\phi_m = 1 + \beta\xi. \tag{21}$$

The traditional value $\beta = 4.7$ was determined from the Kansas atmospheric surface-layer observations (Businger et al., 1971). Slightly higher values are suggested by more recent field measurements (Högström, 1988; Howell and Sun, 1999).

We seek a consistency condition in terms of Ri_f rather than ξ, since the former is suitable for both surface-bounded and free shear flows. Taking $P = u_\star^2 \mathrm{d}U/\mathrm{d}z$ and utilizing (18) and (19), it can be shown that

$$\xi = \phi_m \mathrm{Ri}_f. \tag{22}$$

Substituting (22) into (21) then gives

$$\phi_m = 1/(1 - \beta \mathrm{Ri}_f), \tag{23}$$

which, when reinserted into (22), gives

$$\xi = \frac{\mathrm{Ri}_f}{1 - \beta \mathrm{Ri}_f}. \tag{24}$$

Differentiating (24) then yields

$$\mathrm{d}\xi = \frac{\mathrm{dRi}_f}{(1 - \beta \mathrm{Ri}_f)^2}. \tag{25}$$

These expressions will be used to map $z = \xi L$ to Ri_f in the derivation to follow. From (24), $\xi \to \infty$ corresponds to $\mathrm{Ri}_f \to 1/\beta$. The domain space of our consistency condition is therefore $0 \leq \mathrm{Ri}_f \leq 1/\beta$. Using the traditional value $\beta = 4.7$ gives an upper limit $\mathrm{Ri}_f = 0.213$.

3. Consistency Condition – Stable Case

3.1. Derivation

Our derivation is analogous to that outlined in Section 2.2, but using (18) instead of (13). Inserting (12) and (18) into (8) and substituting into (10) gives

$$\epsilon = \left(\frac{u_\star^3}{kz}\right)\phi_m(1 - \mathrm{Ri}_f). \tag{26}$$

Substituting (12), (18) and (26) into (4) then yields

$$E = u_\star^2 c_{m,LE}^{-1/2}(1 - \mathrm{Ri}_f)^{1/2}. \tag{27}$$

Regarding (26) and (27), note first that $c_{m,LE}$ rather than $c_{m,0}$ (see (16)) appears, since we now account for stability. Because of the local equilibrium assumption, $\mathrm{Ri}_{f,LE}$ rather than Ri_f should likewise appear in these and equations to follow in this section. To simplify the appearance of the equations, however, we defer until Section 4 explicit use of this notation. Secondly, it is seen from (27) that E is a function Ri_f, which since this is a non-linear function of z implies a non-zero transport term in (7). This leads to an inconsistency with the local equilibrium assumption. Evaluation (Appendix B) of the TKE-transport term *a posteriori* using (26) and (27), however, shows that the transport term is less than 1% of total production, $P(1 - Ri_f)$. The inconsistency with local equilibrium is thus negligible.

Proceeding with the derivation, rearranging the steady form of (11) for local equilibrium conditions gives

$$c_{\epsilon 2} - c_{\epsilon 1} = \frac{1}{\sigma_\epsilon}\frac{E}{\epsilon^2}\frac{d}{\mathrm{d}z}\left(K_m\frac{\mathrm{d}\epsilon}{\mathrm{d}z}\right). \tag{28}$$

By then substituting into (28)

1. (20), (26) and (27),
2. (23) for ϕ_m,
3. (24) and (25) to map $z = \xi L$ to Ri_f,

the equation expands to

$$c_{\epsilon 2} - c_{\epsilon 1} = \left(\frac{k^2 c_{m,LE}^{-1/2}}{\sigma_\epsilon}\right) \frac{(1-\beta \mathrm{Ri}_f)^2}{(1-\mathrm{Ri}_f)^{3/2}} \cdot \mathrm{Ri}_f^2 \cdot \left[\frac{d}{d\mathrm{Ri}_f}\left((1-\beta \mathrm{Ri}_f)^3 \frac{d}{d\mathrm{Ri}_f}\left(\frac{1-\mathrm{Ri}_f}{1-\beta \mathrm{Ri}_f}\right)\right) - \frac{d}{d\mathrm{Ri}_f}\left(\frac{(1-\mathrm{Ri}_f)(1-\beta \mathrm{Ri}_f)}{\mathrm{Ri}_f}\right)\right]. \quad (29)$$

Working out the derivatives within the bracketed factor $[\cdot]$ in (29) gives $\mathrm{Ri}_f^2[\cdot] = 1 - \beta^2 \mathrm{Ri}_f^2 = (1-\beta \mathrm{Ri}_f)(1+\beta \mathrm{Ri}_f)$, reducing the equation to

$$c_{\epsilon 2} - c_{\epsilon 1} = \frac{k^2 c_{m,LE}^{-1/2}}{\sigma_\epsilon} \left[\frac{(1-\beta \mathrm{Ri}_f)^3 (1+\beta \mathrm{Ri}_f)}{(1-\mathrm{Ri}_f)^{3/2}}\right]. \quad (30)$$

Equation (30) is the sought consistency condition, again valid only for $0 \leq \mathrm{Ri}_f \leq 1/\beta$. Since the bracketed factor on the right side equals one and $c_{m,LE} = c_{m,0}$ for $\mathrm{Ri}_f = 0$, (17) is recovered for neutral conditions. In general, however, the right side of (30) is a function of Ri_f. Constant values of $c_{\epsilon 1}$ and $c_{\epsilon 2}$, though, render the left side constant, independent of Ri_f. *This shows that (11) as standardly applied is inconsistent with MO theory.*

3.2. Effects of inconsistency

The effects of the inconsistency can be understood by first considering the neutral case, where consistency is enforced by using (17) to set the value of σ_ϵ. This specification controls the magnitude of the transport term in (11), which in the surface layer is a source owing to ϵ flux convergence in the layer. Specifically, using (17) to set the value of σ_ϵ enforces exact balance between the transport source and net local sink from the production and dissipation terms in (11) implied in local equilibrium by the specification $c_{\epsilon 2} > c_{\epsilon 1}$. The transport source and local sink terms are represented non-dimensionally by the right and left sides of (17), respectively. The balancing of the two in neutral conditions by appropriately setting σ_ϵ thus ensures consistency with the steady-state assumption of surface-layer theory. This, along with proper representation of turbulence profiles near the upper edge of the boundary layer (Freedman and Jacobson, 2002), leads to generally accurate computation by (11) of neutral boundary layers as a whole, since turbulence dynamics in their outer portions are largely (i.e. in the traditional case of weak to moderately strong outer layer mean forcing and laminar/quasi-laminar upper boundary conditions) similar to those in the surface layer.

To see the effects of the inconsistency for the stable case, we rewrite the generalized expression, (30), as $1 = \tilde{T}_\epsilon \equiv (c_{m,0}/c_{m,LE})^{1/2} f_\epsilon$, where f_ϵ is the bracketed

factor on the right side of (30) and (17) was used to eliminate remaining parameters. $\tilde{T}_\epsilon$ is thus the Ri_f-dependent part of the non-dimensional ϵ-transport term in the stable surface layer, normalized to equal one in neutral conditions. We plot the quantity in Figure 1 using (A6) and the more commonly used MY82 model for $c_{m,LE}$. For the former, we plot up to $\mathrm{Ri}_f = 1/\beta = 0.213$ ($\beta = 4.7$), the upper domain limit of f_ϵ, whereas in the latter we plot up to $\mathrm{Ri}_f = 0.19$, the approximate value of $\mathrm{Ri}_{f,c}$ (the upper domain limit of $c_{m,LE}$, see Appendix A) in MY82's model. As stated before, the dependency of $\tilde{T}_\epsilon$ on Ri_f (seen graphically now) leads to an inconsistency with MO theory, since the left side of (30) does not depend of Ri_f. Specifically, however, the fact that (for both $c_{m,LE}$ models) $\tilde{T}_\epsilon$ *decreases* strongly with Ri_f indicates a strong reduction with stability of the ϵ-transport term. This is a consequence of (25), from which $d/\mathrm{d}z \sim d/\mathrm{d}\xi = (1 - \beta \mathrm{Ri}_f)^2 d/\mathrm{dRi}_f \to 0$ as $\mathrm{Ri}_f \to 1/\beta$. Because of this reduction, the transport term in (11) becomes more and more unable (with increased stability) to balance the net sink from the local terms resulting from $c_{\epsilon 2} > c_{\epsilon 1}$. This leads to a net ϵ sink, inconsistent with the steady-state assumption of surface-layer theory, and we believe in turn to the strongly time-decreasing ϵ and large K_m and K_h ($\propto 1/\epsilon$) found in previous applications of (11) to the 1D-SBL.

4. Development of MO-Consistent ϵ-Equation

Since the ϵ-transport term is decreasingly unable with increased stability to provide the ϵ necessary for bounded turbulence in the stable surface layer and apparently 1D-SBL, attempts at rectifying the problem should be directed at altering the local production and/or dissipation terms in (11) in such a manner to incorporate an additional ϵ source with increased stability. This has been the strategy used to produce modified forms of (11) in the previous investigations referenced in Section 1. Here, we produce a similar modification by explicitly using (30) to enforce consistency with MO theory

Consistency of (11) with MO theory is enforced by solving (30) for either $c_{\epsilon 1}$ or $c_{\epsilon 2}$. Solving for σ_ϵ, as done for the neutral case using (17), would demand that this approach zero as Ri_f approaches $1/\beta$, unreasonable since this implies an approach towards infinite ϵ transport. Carrying out the solution for $c_{\epsilon 1}$ thus gives

$$c_{\epsilon 1}(\mathrm{Ri}) = c_{\epsilon 2} - \frac{k^2 c_{m,LE}^{-1/2}}{\sigma_\epsilon}\left[\frac{(1 - \beta \mathrm{Ri}_{f,LE})^3 (1 + \beta \mathrm{Ri}_{f,LE})}{(1 - \mathrm{Ri}_{f,LE})^{3/2}}\right], \tag{31}$$

where the notation $\mathrm{Ri}_f = \mathrm{Ri}_{f,LE}$ is now explicitly used. Through (A6) and (A8), enforcement of consistency thus leads to an Ri dependence in this parameter. An analogous dependence in $c_{\epsilon 2}$ is obtained if enforced through that parameter. The effect of the dependencies on turbulence development, however, would be different since $c_{\epsilon 1}$ multiplies $P + B$, zero in isotropic turbulence ($\overline{uw} = 0$, $\overline{w\theta} = 0$), whereas

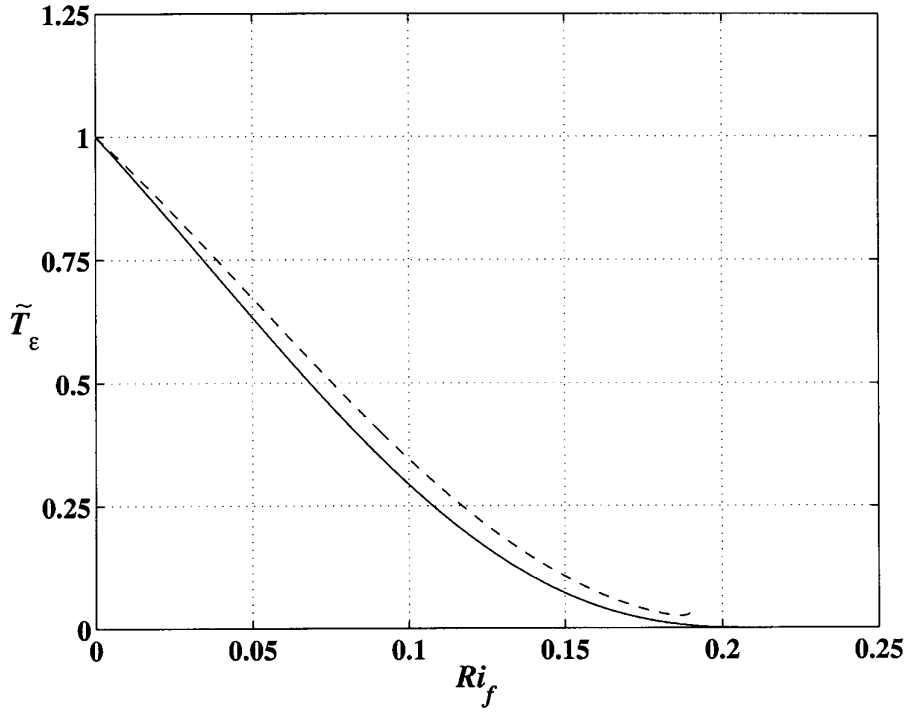

Figure 1. $\tilde{T}_\epsilon \equiv (c_{m,0}/c_{m,LE})^{1/2} f_\epsilon$ vs. Ri_f, where f_ϵ is the bracketed factor on the right side of (30). Solid, $c_{m,LE}$ from (A6); dashed, $c_{m,LE}$ from Mellor and Yamada (1982) Level-2 model. See text for further explanation.

$c_{\epsilon 2}$ multiplies ϵ, nonzero in isotropic turbulence. Since the MO analysis basing our modification applies to anisotropic turbulence, due to preferential streamwise TKE production from the mean shear and vertical TKE suppression from the mean stratification, we felt it best to restrict the effects of the modification only to this case, not affecting isotropic turbulence. We therefore enforce consistency through $c_{\epsilon 1}$ rather than $c_{\epsilon 2}$.

We maintain $c_{\epsilon 2} = 1.92$ and $\sigma_\epsilon = 1.1$. With these, the value $\sigma_E = 1.6$ is then set to give $\kappa \equiv c_{\epsilon 2}\sigma_\epsilon/\sigma_E = 1.3$, necessary for accurate prediction of the neutral ABL (Freedman and Jacobson, 2002). With $c_{m,0} = 0.115$ from (A6),* this yields $c_{\epsilon 1}(0) = 1.51$. Although higher than the standard engineering value $c_{\epsilon 1} = 1.44$, the difference $c_{\epsilon 2} - c_{\epsilon 1}$ remains adequate for reasonable predictions of turbulence

* This is higher than the typical engineering value 0.09, a result of GL78's procedure for calibrating closure parameters in their SOC. The value is also much greater than $\sim$ 0.03 required to capture the much lower $-\overline{uw}/E$ measured in atmospheric relative to laboratory neutral surface layers. Inclusion of GL78's wall parameterization helps rectify this as well as the lower neutral value of turbulence Prandtl number, $\mathrm{Pr}_{t,0} = c_{m,0}/c_{h,0} = 2/3$, predicted by (A6) and (A7) compared to that ($\sim$ 1) measured in atmospheric surface layers (Högström, 1988).

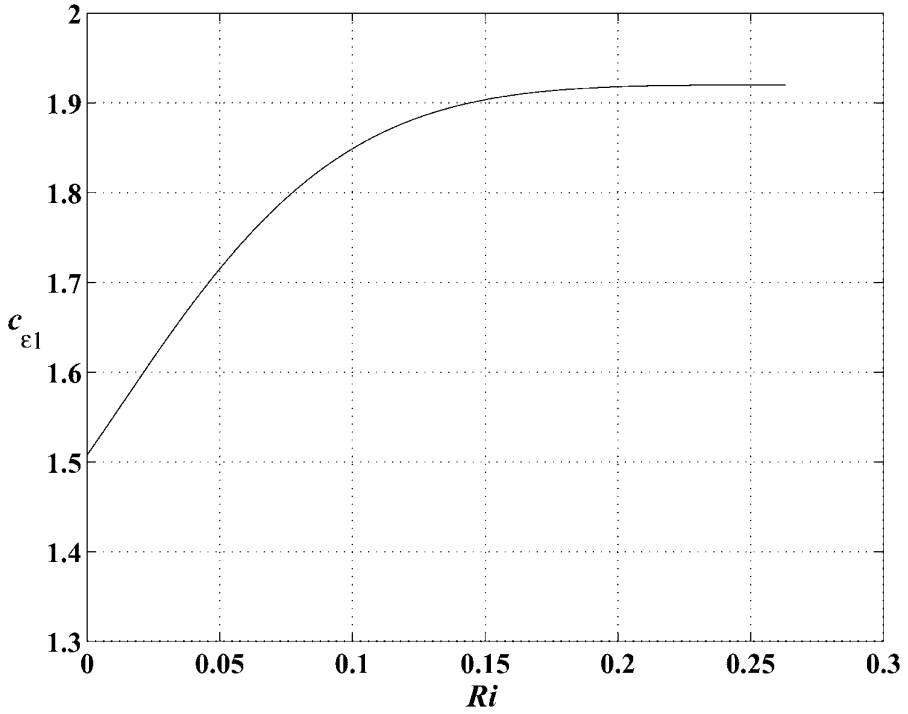

Figure 2. $c_{\epsilon 1}$ vs. Ri, computed from (31).

growth rates in neutral free shear flows (Durbin and Pettersson-Reif, 2001). We employ the traditional value $\beta = 4.7$ in (31), with $c_{m,LE}$ and $\mathrm{Ri}_{f,LE}$ computed as a function of Ri from (A6) and (A8), respectively. The equation is then substituted for $c_{\epsilon 1}$ in (11) to yield a form consistent with MO theory.

A plot of (31) is shown in Figure 2. The increase of $c_{\epsilon 1}$ with Ri suggests increasing relative (per unit total TKE production) local ϵ production with increasing stability. The variation thus reflects the additional local ϵ source necessary to balance the stable surface layer TKE budget, in turn hypothesized necessary for bounded turbulence in the 1D-SBL. Although other modifications producing an additional source have been proposed in the aforementioned previous investigations, the advantage of ours is that the source is implemented gradually with increasing stability in a manner consistent with established theory. On a practical level, the leveling off $c_{\epsilon 1} \rightarrow c_{\epsilon 2}$ as $\mathrm{Ri}_{f,LE} \rightarrow 0.213$ (corresponding to Ri = 0.263 from (A8)) suggests $c_{\epsilon 1} = c_{\epsilon 2}$ for $\mathrm{Ri}_{f,LE} > 0.213$, which we employ in application (Section 5).

Finally, if the effects of shear and buoyancy are separated in (11) by including a parameter $c_{\epsilon 3}$ multiplying the buoyancy term, it can be shown that (30) changes to

$$c_{\epsilon 2} - c_{\epsilon 1}\left(\frac{1 - c_{\epsilon 3}\mathrm{Ri}_f}{1 - \mathrm{Ri}_f}\right) = \frac{k^2 c_{m,LE}^{-1/2}}{\sigma_\epsilon}\left[\frac{(1 - \beta\mathrm{Ri}_f)^3(1 + \beta\mathrm{Ri}_f)}{(1 - \mathrm{Ri}_f)^{3/2}}\right]. \tag{32}$$

It is seen that simply setting $c_{\epsilon 3}$ to a constant value (various ones have been used, see Baumert and Peters (2000)) does not remove the need to enforce consistency, since the functionalities of Ri_f on the left and right sides of (32) are not identical. Seeing this, we simplified matters by setting $c_{\epsilon 3} = 1$, eliminating the factor multiplying $c_{\epsilon 1}$ on the left side, and directed consistency enforcement towards absorbing the functionality on the right side into $c_{\epsilon 1}$.

5. Application to 1D-SBL

We turn now to the 1D-SBL predictions of our modification. Of particular interest is its ability to yield a 'quasi-steady' solution (hereafter the QSSBL), characterized by steady boundary-layer depth, surface drag variables, and mean wind and turbulence profiles in the main body of the boundary layer. The unsteadiness is manifested only in the continual cooling of the boundary layer (vertical Θ gradients, however, are approximately steady) and in phenomena near the boundary-layer top (e.g., inertial oscillation of the mean wind). Such a solution is readily converged to by models employing algebraic l formulations (Brost and Wyngaard, 1978; Lacser and Arya, 1986) as well as by large-eddy simulation (LES) (Brown et al., 1994; Kosovic and Curry, 2000), with many features deducible from the analytical solutions of Nieuwstadt (1985) and Derbyshire (1990). Often long turbulence time scales in stable atmospheric field conditions, however, lead to large times (on the order of several hours) to reach a quasi-steady state, and for this reason other processes, associated for example with terrain, surface heterogeneity, mesoscale motions and waves, may strongly affect or dominate a given field SBL. Although the QSSBL is thus probably never strictly observed in the field (Derbyshire, 1995; Mahrt, 1999), select field observations (e.g., Nieuwstadt, 1984) support its relevance to SBLs found in the field. As such, the case is a useful benchmark to assess turbulence model predictions for stable atmospheric application, and is particularly useful here since previous applications of (11) using constant values of closure parameters have failed to yield this solution, giving instead unphysical predictions associated with continually growing turbulence.

5.1. Design

Model solutions are obtained by finite-difference numerical integration on a staggered vertical grid (mean quantities held at grid layer midpoints and turbulence

quantities at grid levels). The lower boundary condition on (3) is externally specified through $F_0 = g/\Theta_a(\overline{w\theta})_0 < 0$. For (1) and (2), surface Reynolds stresses, $(\overline{uw})_0$ and $(\overline{vw})_0$, are computed by first solving the cubic for $u_\star$ that results from integrating (18) from z_0 to h_2 and $W(z_0) = 0$ to $W(h_2) = W_2$,

$$\frac{u_\star^3}{u_{\star,0}} - u_\star^2 + \frac{\beta F_0(h_2 - z_0)}{W_2} = 0, \tag{33}$$

where (19) and (21) were used. Here, $W \equiv (U^2 + V^2)^{1/2}$ is the wind speed (interchangeable with U in Section 2.3), z_0 is the surface roughness length (externally specified), h_2 the midpoint of the grid layer adjacent to the surface, and $u_{\star,0} = kW_2/\ln(h_2/z_0)$.* Surface Reynolds stresses are then computed via $(\overline{uw})_0 = -u_\star^2\cos(\alpha_0)$ and $(\overline{vw})_0 = -u_\star^2\sin(\alpha_0)$, where $\alpha_0 = \tan^{-1}(V_2/U_2)$ is the mean wind direction at h_2.

The lower boundary condition on E is computed from (16), to which (27) collapses at $\mathrm{Ri}_f = 0$ ($z = 0$). That for ϵ is specified by computing its vertical flux at h_2,

$$-\left(\frac{K_m}{\sigma_\epsilon}\frac{\partial\epsilon}{\partial z}\right)\bigg|_{h_2} = \frac{u_\star^4}{\sigma_\epsilon h_2(1 + \beta h_2/L)}, \tag{34}$$

derived by substituting (20)–(22) and (26) into the left side of (34). For upper boundary conditions, we specify $E = 10^{-9}$ m^2 s^{-2} and $\epsilon = 10^{-13}$ m^2 s^{-3} at the computational domain top, H, and $U = G$, $V = 0$ and $\Theta = \Theta_a$ a half grid distance below H.

We employ 118 levels to $H = 5$ km with $\Delta z = 10$ m adjacent to the surface, stretching to $\Delta z \approx 20$ m at $z \approx 500$ m. This places roughly 30 levels in the region $z < 500$ m, where the bulk of boundary-layer development takes place in our cases (the additional layers above are needed to accommodate the neutral ABL initializing the simulations). Central space differencing is employed to compute diffusion terms. Values of K_m and K_h for evaluating these in (1)–(3) are weighted averages of values at the grid level and at the two adjacent layer midpoints, weighted by 0.8 at the level and 0.1 at the midpoints. This was found necessary for numerical stability in the Θ profile near the boundary-layer top, where an inflection point develops over time (see, for example, Figure 4b, solid line at $z \approx 150$ m). Like terms in (7) and (11), on the other hand, employ values of K_m computed only at layer midpoints, the location of TKE and ϵ fluxes. First-order implicit time advancement is used with $\Delta t = 5$ s. Values of $g = 9.81$ m s^{-2} and $\Theta_a = 300$ K are specified.

The computational cases (Table I) are characterized by increasing values of F_0 and corresponding case-to-case increase in surface cooling rate and stratification. We also list the ratio $F_0/F_{\max}$, where $F_{\max} = \mathrm{Ri}_f G^2|f|/\sqrt{3}$ is a theoretical

* It can be shown that the physical root of (33) is in the range $(2/3)u_{\star,0} \le u_\star \le u_{\star,0}$ provided $\beta F_0(h_2 - z_0)/W_2 \le (4/27)u_{\star,0}^2$, satisfied in our computational cases. No physical root exists when this inequality is not satisfied.

TABLE I
Computational cases and bulk predictions at $t = 8$.[a]

Case	F_0 (m^2 s^{-3})	$F_0/F_{\max}$	$u_\star$ (m s^{-1})	α_0 (deg)	h (m)
A	2.7×10^{-4}	0.22	0.349	31.7	409
B	5.0×10^{-4}	0.41	0.290	36.9	214
C	6.0×10^{-4}	0.49	0.260	39.0	160
D	8.0×10^{-4}	0.65	0.200	43.6	88
E	1.0×10^{-3}	0.81	0.163	46.7	52

[a] $G = 10$ m s^{-1}, $f = 10^{-4}$ s^{-1}, $z_0 = 0.10$ m for each case. See text for definition of symbols.

absolute upper limit supporting a QSSBL (Derbyshire, 1990). In all cases, $G = 10\,\mathrm{m\,s^{-1}}$, $f = 1.0 \times 10^{-4}\,\mathrm{s^{-1}}$ and $z_0 = 0.1$ m. A value $\mathrm{Ri}_f = 1/\beta = 0.213$ is used to compute $F_{\max}$, a choice whose reasoning will be apparent from Section 5.2.2. Initial profiles were obtained from the final results of a three hour neutral integration ($F_0 = 0$) starting from uniform profiles $U(z) = G$, $V(z) = 0$, $\Theta(z) = \Theta_a$, $E(z) = 10^{-9}\,\mathrm{m^2\,s^{-2}}$ and $\epsilon(z) = 10^{-13}\,\mathrm{m^2\,s^{-3}}$. After this (designated $t = 0$), F_0 was set to the appropriate fixed value for a given case and computations proceeded for eight hours (designated $t = 8$).

5.2. RESULTS

5.2.1. *Approach to Quasi-Steady State*

Time plots of predicted boundary-layer depth, h, surface friction velocity, $u_\star$, and surface-layer mean wind direction, α_0, for each case are shown in Figure 3. Here, $h = h_\theta/0.95$ with h_θ the height at which $\overline{w\theta}$ falls to 5% of its surface value. Values at $t = 0$ are those after the three-hour neutral integration initializing the runs; $h = 0$ at $t = 0$ is therefore a consequence of defining h in terms of $\overline{w\theta}$. It is seen that predictions correctly converge to an approximate steady-state by $t = 8$; the predicted values at this time are listed in Table I. Computations made by us with $c_{\epsilon 1}$ held constant, on the other hand, fail to converge to a steady-state, giving instead completely unphysical results associated with growing turbulence, in concurrence with previous applications. These computations are not shown for brevity.

The associated approach to steady-state of profiles of mean quantities, W and Θ (shown dimensionally to convey overall magnitudes), and turbulence fluxes, $\tau_m \equiv (\overline{uw}^2 + \overline{vw}^2)^{1/2}$ and $\overline{w\theta}$, for case C are shown in Figures 4 and 5, respectively. The development of a wind speed maximum atop the boundary layer (Figure 4a) appears reasonable and the transition of the Θ profile from a concave to convex shape (Figure 4b) is consistent with expectations for a turbulence, rather that radiatively, driven SBL (André and Mahrt, 1982). Concerning fluxes, fits to

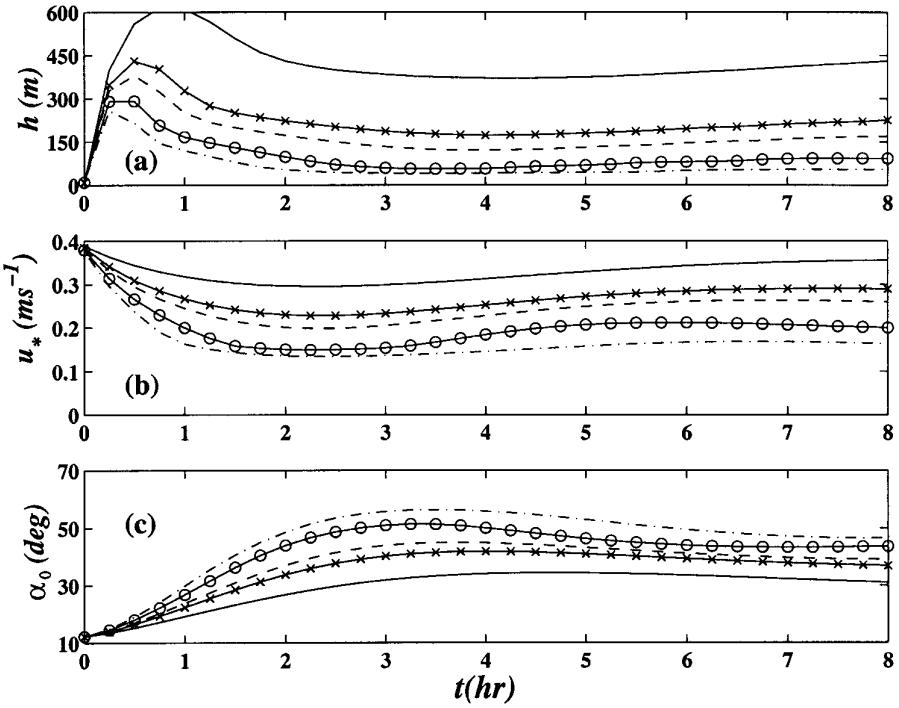

Figure 3. Time plots of model-predicted (a) boundary-layer depth, (b) surface friction velocity and (c) surface-layer mean wind direction. Solid, case A; solid-×, case B; dashed, case C; solid-○, case D; dashed-dot, case E.

field observations as well as theoretical predictions of Nieuwstadt (1985) suggest $\tau_m/u_\star^2 = (1 - z/h)^m$ and $\overline{w\theta}/(\overline{w\theta})_0 = (1 - z/h)^n$, where m and n are constants. Sorbjan (1989), fitting these to the Minnesota field data (Caughey et al., 1979), representative of an early evening, evolving SBL, deduced $m = 2$ and $n = 3$, i.e., concave profiles. Grant (1997) also found concave shapes in his early-evening field data. Nieuwstadt's theory, on the other hand, valid for a QSSBL, predicts $m = 3/2$ and $n = 1$; profiles with these exponents are plotted as the dashed-dot lines in Figure 5. Taken together, these findings support evolution towards less concave flux profile shapes, a behaviour with which our predictions are consistent. Profile behaviour of cases not shown is similar to that just described.

We note that similar predictions at $t = 8$ were found from runs made with the Level-2.5 model for stability functions replaced with a constant, typical engineering value $c_m = c_{m,LE} = c_h = c_{h,LE} = 0.09$. This leads to $\mathrm{Ri}_{f,LE} = \mathrm{Pr}_{t,LE}^{-1}\mathrm{Ri} = \mathrm{Ri}$ (since $\mathrm{Pr}_{t,LE} = c_{m,LE}/c_{h,LE} = 1$) for use in (31) and to the typical engineering value $c_{\epsilon 1}(0) = 1.44$ from solving the equation for neutral conditions. These runs were performed to examine the change in results if our SOC model was replaced with constant, user-specified values of stability functions, more common

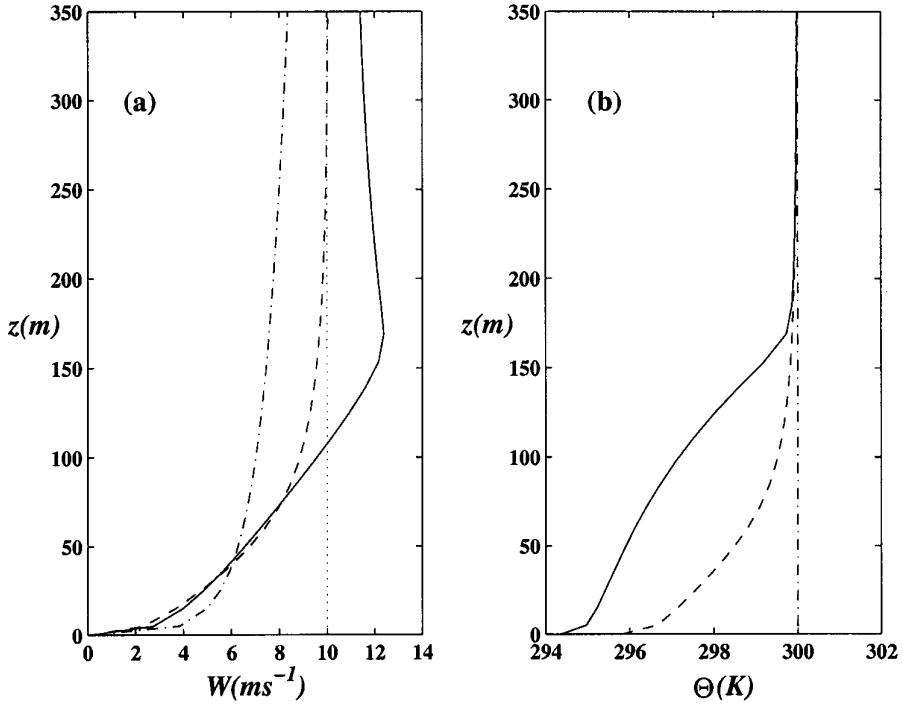

Figure 4. Model-predicted profiles (case C) of mean (a) wind speed and (b) potential temperature. Dashed-dot, $t = 0$; dashed, $t = 4$; solid $t = 8$. Dotted line in (a) denotes geostrophic wind speed.

in practical engineering use of 'two-equation' (i.e. for TKE and turbulence scale) turbulence models. Since similar quasi-steady predictions were obtained, the arrival at steady-state thus appears not to depend on the use of SOC, but rather on proper representation of physics in (11). The only major difference appeared in the approach to steady-state, where with this constant stability function value the early-time h values were roughly twice those obtained with our Level-2.5 model (shown for the latter at $t \lesssim 1$ in Figure 3a). The use of SOC may thus be important in accurately predicting the approach to steady-state. Specifying different values of stability functions than used here may, however, bring the early-time evolution of runs with constant stability functions closer to that shown in Figure 3.

5.2.2. *Consistency with Nieuwstadt's Analytical Solutions*

To this point, we have made passing allusion to Nieuwstadt's analytical profiles of the QSSBL. We now pursue further the consistency of our predictions with these. The analytical solutions are derived from the steady form of (1) and (2) and unsteady form of (3) under constant G and f. The key assumption allowing a solution is a height-invariant Ri and Ri_f (we call the latter $\mathrm{Ri}_{f,\infty}$). By imposing these to the surface, thereby not allowing Richardson numbers to approach zero

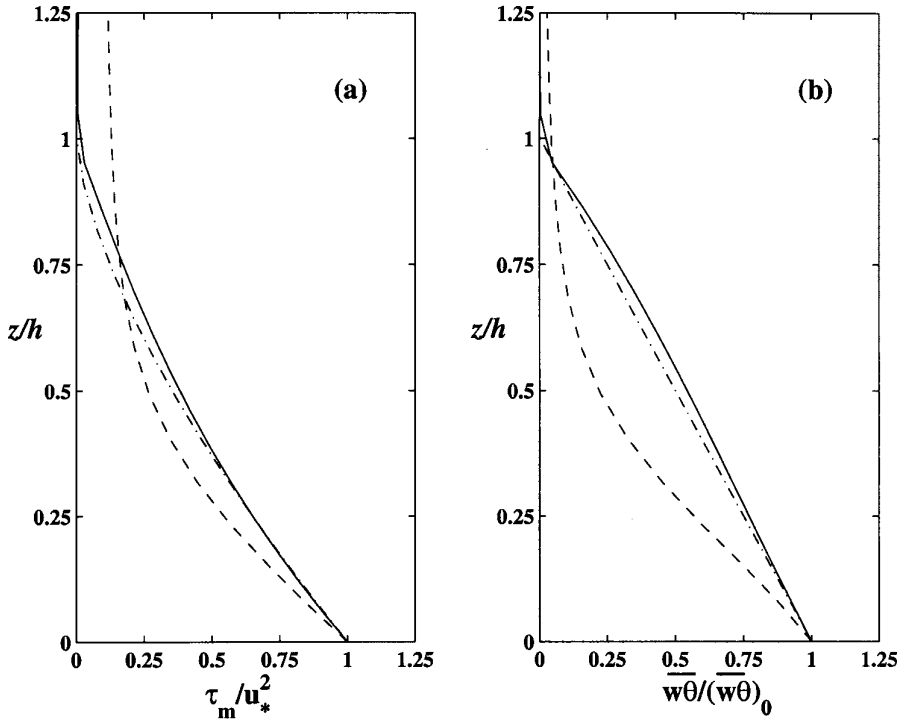

Figure 5. Model-predicted profiles (case C) of non-dimensional (a) turbulent momentum flux magnitude and (b) turbulent heat flux. Dashed, $t = 4$; solid, $t = 8$; dashed-dot, Nieuwstadt's theoretical predictions.

at the surface as MO theory demands, the profiles become representative of the QSSBL in the 'strong-stability' limit $L/h \to 0$. It is in this limiting sense that the parameter $F_{\max}$ in Table I applies. To generalize for weak to moderate stabilities, the profiles therefore need to be matched to MO theory in the mutual limit $z/h \to 0$ and $\xi \to \infty$. Matched profiles for key variables are given in Nieuwstadt (1985) while Derbyshire (1990) addresses others. From this matching, it is apparent that $\mathrm{Ri}_{f,\infty} = 1/\beta$ (the value from MO theory as $\xi \to \infty$); the value 0.2 imposed by Nieuwstadt (1985) is consistent with typical β values. Aside from the need for matching, another weakness of the constant $\mathrm{Ri}/\mathrm{Ri}_f$ assumption is that it cannot capture effects near the boundary-layer top, where Richardson numbers generally increase to large values due to the local wind speed maximum often found there. In fact, the constant $\mathrm{Ri}/\mathrm{Ri}_f$ assumption, coupled with the use of completely laminar upper boundary conditions (zero Reynolds stresses and heat flux at $z = h$), leads to singularities in analytical mean profiles at $z = h$. For the purpose of comparing to model results, the solutions are therefore most appropriate (if matched to MO

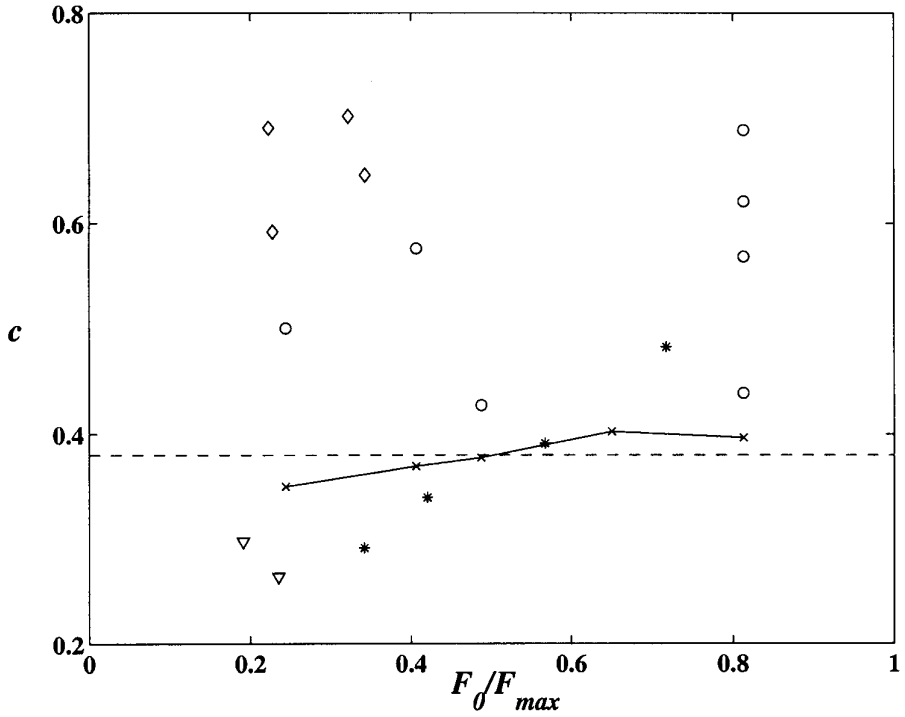

Figure 6. Plot vs. $F_0/F_{\max}$ of non-dimensional boundary-layer depth $c = h(f/u_\star L)^{1/2}$; (-x) model predictions ($t = 8$); (○) Brown et al. (1994) LES results; (∗) Kosovic and Curry (2000) LES results; (▽) Lenschow et al. (1988) field data; (◇) Caughey et al. (1979) field data. Dashed line is $c = 0.38$, predicted by Nieuwstadt's theory. See text for discussion.

theory) in the surface layer and main body of the QSSBL. Full details of the theory are available in Nieuwstadt (1985), Derbyshire (1990) and Garratt (1992).

Predictions of non-dimensional boundary-layer depth, $c = h(f/u_\star L)^{1/2}$, by our model are shown in Figure 6 (solid-x line). Nieuwstadt's theory predicts $c = (\sqrt{3}k\mathrm{Ri}_{f,\infty})^{1/2}$; taking $\mathrm{Ri}_{f,\infty} = 1/\beta = 0.213$ and $k = 0.4$ gives $c = 0.38$. It is seen that model predictions agree very well with this theoretical value, with slight increase with stability apparent (also apparent in the LES results shown in the figure). In Figure 7 we show predicted profiles of the non-dimensional eddy viscosity, $K_m/u_\star L$, for cases A, C and E. Nieuwstadt's theory, matched to MO theory at the surface, predicts

$$\frac{K_m}{u_\star L} = \frac{(kz/L)(1 - z/h)^2}{1 + \beta z/L}. \tag{35}$$

The theoretical profiles for each case (generated by plugging the predicted L at $t = 8$ for each case into (35)) are also plotted in the figure. Again, good correspondence between model predictions and theory is seen, although less so for case

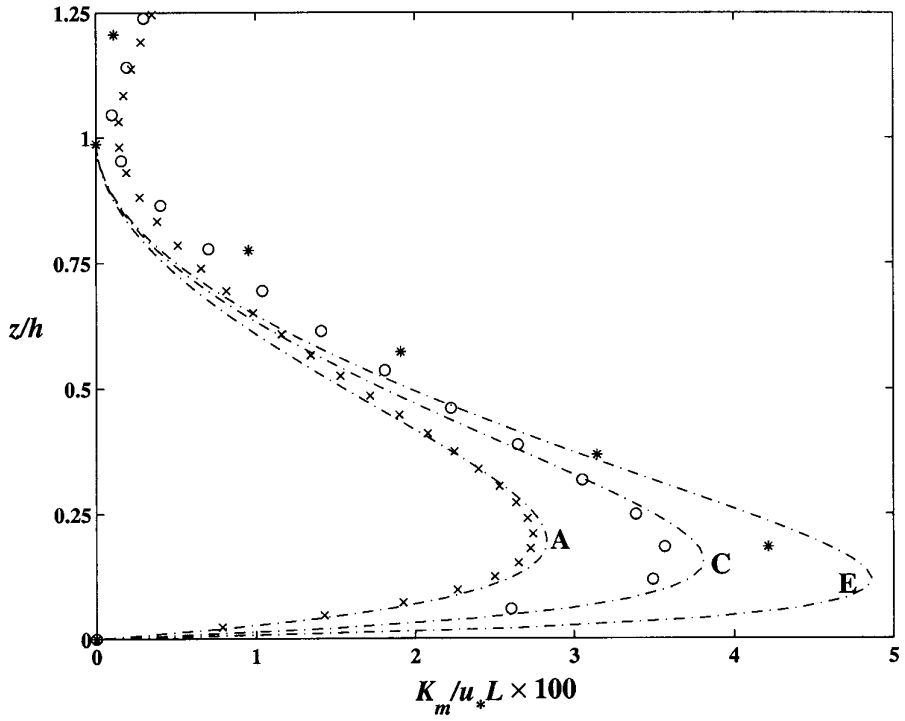

Figure 7. Model-predicted profiles ($t = 8$) of non-dimensional eddy viscosity. ($\times$) case A; ($\bigcirc$) case C; ($*$) case E. Nieuwstadt's theoretical expression, (35), for each case (as noted) plotted as dashed-dot lines.

E since, as seen in the figure, the grid is too course to resolve the lower part of the analytical profile. The theoretical solution for non-dimensional K_h is analogous to (35), but with the denominator replaced by $Pr_{t,0} + \beta z/L$, where $Pr_{t,0}$ is the neutral surface layer value of Pr_t. Our predictions (not shown) likewise agree well with this theoretical expression in spite of the overly low model value of $\mathrm{Pr}_{t,0}$ (see footnote 1). Theoretical agreement is also seen in quasi-steady profiles of vertical fluxes (Figure 5) as well as in those for other variables (e.g., E and ϵ, not shown).

The strong agreement of model predictions with Nieuwstadt's theory suggests that this is not a coincidence but instead a result of overlap of the model formulation with the theory. We believe this overlap results in some way from our explicit implementation of (21) into the model. This first allows the near-surface solutions of the model and theory (if MO-matched) to be consistent. Secondly, and perhaps more importantly, since (21) implies $\mathrm{Ri}_f \to 1/\beta$ for $\xi \to \infty$, the approach to constant $\mathrm{Ri}/\mathrm{Ri}_f$ in the body of the QSSBL underlying Nieuwstadt's theory is apparently incorporated into the model design. Derbyshire (1995, 1999) also reports strong agreement of 1D model results with idealized theories. While this does not

necessarily imply predictive *accuracy* (addressed in the next subsection), it does lend a desirable coherence and understandability to model predictions.

5.2.3. *Accuracy of Predictions*

It was established in the previous subsection that quasi-steady predictions non-dimensionally coincide very closely with Nieuwstadt's theory. The accuracy of predictions thus relies on (a) the accuracy of Nieuwstadt's theory in describing the QSSBL and (b) the accuracy of predictions of $u_\star$, the only internal variable in the non-dimensionalization. Assuming the first, the second assures correct translation from non-dimensional to dimensional accuracy.

Predictions of the geostrophic drag coefficient, $C_g = (u_\star/G)^2$, and surface-layer mean wind direction, α_0, plotted against $\mu_0 = ku_\star/fL$, are shown in Figure 8. Also shown are several LES predictions, field data of Caughey et al. (1979) and Lenschow et al. (1988), and Rossby-number similarity relationships of Arya (1975). The empirical functions $A(\mu_0)$ and $B(\mu_0)$ in Arya's relationships are formed from fitting the Wangara data, thereby indirectly supplying additional field data to the comparison. Since μ_0 involves $u_\star$ in its definition, the assessment of accurate $u_\star$ prediction unfortunately is not made with respect to a fully external variable. Also, the scatter in the LES (probably due to the different subgrid parameterizations and domain sizes used among these) and field data warrants some uncertainty in using these to deduce model accuracy. Nonetheless, it is seen that our predictions broadly reproduce the decrease (increase) of C_g (α_0) with stability found in the data. Slight overall underprediction of turbulence effects (lower C_g, higher α_0), more so with respect to LES, is suggested.

Concerning the accuracy of Nieuwstadt's theory, the above mentioned scatter in SBL LES and field data also hampers this assessment. This is seen in Figure 6 for non-dimensional boundary-layer depth, c, in which the data scatter is too large to confirm the theoretical value (dashed line). The range of c values among these data is similar to that reported in Brown et al. (1994). Field profiles of non-dimensional eddy viscosity from Nieuwstadt (1984) and Lenschow et al. (1988) (redrawn from data presented in these papers) are plotted in Figure 9 along with the case A prediction at $t = 8$, of similar h/L to that of the data. Both sets of field data show smaller overall non-dimensional K_m than predicted by the model (and theory by virtue of Figure 7). Lenschow et al. (1988), however, mention the possibility of terrain-induced wave effects in their data. The Nieuwstadt points reflect averages of roughly 100 profiles taken from the Cabauw tower. A fairly substantial variation among profiles, however, is suggested from the bars (representing ± 1 standard deviation from the average) drawn around the points in Nieuwstadt's (1984) figures. Based on this, it is difficult to say whether the implied overprediction of non-dimensional K_m by model and theory is real or whether the smaller values in both data profiles is a coincidental occurrence within the natural variability of SBL field data (Derbyshire, 1995). Given the near impossibility of 'clean' QSSBL field data (see opening paragraph of this section), further refined LES, direct-numerical sim-

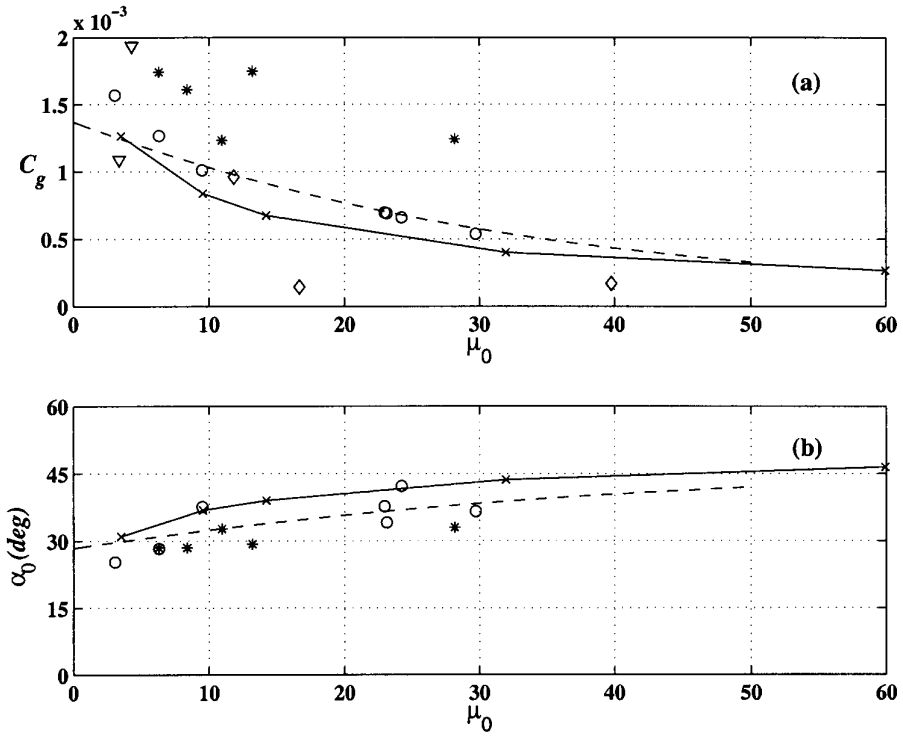

Figure 8. Plots vs. $\mu_0 = ku_\star/fL$ of (a) geostrophic drag coefficient and (b) surface-layer mean wind direction. Symbols as in Figure 6. The dashed lines are Rossby-number similarity relationships of Arya (1975).

ulation (extending the work of Coleman et al. (1992) to higher Reynolds number) and/or laboratory (extending the work of Ohya (2001) to include rotation) results are needed to more clearly determine the accuracy of Nieuwstadt's theory.

6. Conclusion

The central result of this paper is consistency condition (30), which the values of closure parameters in the standard ϵ-equation, (11), must obey for consistency with Monin–Obukhov (MO) similarity theory of the stably-stratified surface layer. The condition was derived by extending the procedure used to derive (17) to account for the MO modification of the mean wind profile. Examination of (30) shows that inconsistency with MO theory results if constant values of closure parameters $c_{\epsilon 1}$ and $c_{\epsilon 2}$ are maintained for all Ri_f, and the large overpredictions of turbulence reported in previous applications of the ϵ-equation to the 1D-SBL are traced to this inconsistency. Consistency, on the other hand, is achieved by absorbing the Ri_f

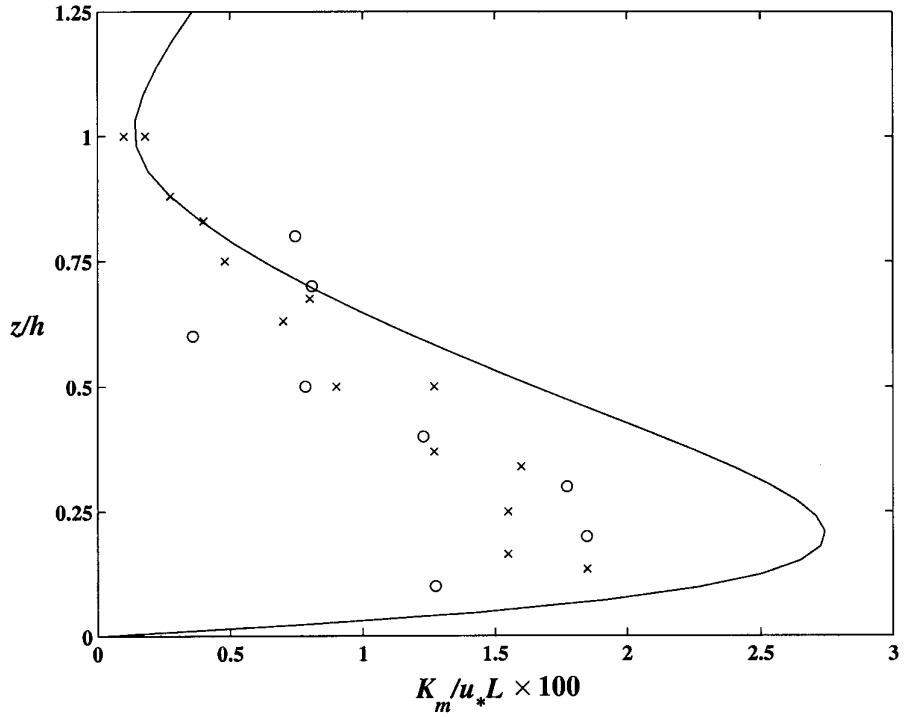

Figure 9. Profiles of non-dimensional eddy viscosity. Solid, case A ($t = 8$); (○) field data of Nieuwstadt (1984); (×) field data of Lenschow et al. (1988). Field data redrawn from figures presented in above papers.

functionality on the right side of (30) into either $c_{\epsilon 1}$ or $c_{\epsilon 2}$. By absorbing it into $c_{\epsilon 1}$ in (31) and reinserting this into (11), a MO-consistent ϵ-equation is produced. The equation is combined with Andrén's (1990) Level-2.5 model (neglecting its wall parameterization) to yield a modified parameterization for vertical eddy viscosity and diffusivities.

The modified model is evaluated by testing (through numerical computation) its ability to reproduce accurately the quasi-steady 1D-SBL (QSSBL). The fact that the model produces a QSSBL is its main success, since previous 1D-SBL applications (as well as ours) of (11) with closure parameters held constant at typical engineering values do not converge to steady-state, giving instead completely unphysical results associated with growing turbulence. This success by itself is an encouraging step towards ultimately replacing algebraic l formulations currently employed in 3D meteorological flow prediction codes with a more generally applicable transport equation for the turbulence scale. Model predictions of the QSSBL non-dimensionally show particularly strong correspondence with Nieuwstadt's (1985) analytical solutions. The broad agreement found in predicted

$u_\star$ (the only internal non-dimensionalizing variable) with respect to field and LES data as well as to Rossby-number similarity relationships then implies dimensional accuracy of model predictions, assuming Nieuwstadt's theory accurately describes the QSSBL. Given the difficulty in obtaining field data strictly valid for a QSSBL, future refined LES, direct-numerical simulation and/or laboratory data are needed to ascertain the latter.

Acknowledgements

The authors thank Drs. A. R. Brown and B. Kosovic for supplying and discussing with us their LES results, as well as Drs. P. A. Durbin and J. A. Ferziger for helpful comments regarding this work. The research was supported by grants from the National Science Foundation and the National Aeronautics and Space Administration under the New Investigator Program (NIP) in Earth Sciences.

Appendix A: Level-2.5 Model for c_m and c_h

Applying the Level-2.5 simplification procedure to GL78's SOC (neglecting its wall parameterization) yields

$$c_m = \frac{\chi_5\chi_4 + \chi_6\chi_2}{\chi_1\chi_4 + \chi_3\chi_2} \tag{A1}$$

$$c_h = \frac{\chi_6 - \chi_3 c_m}{\chi_4}, \tag{A2}$$

where

$$\begin{aligned}
\chi_1 &= 1 + \frac{2(1-c_2)^2}{3c_1^2}G_m - \frac{(1-c_3)}{c_1 c_{1\theta}}G_h \\
\chi_2 &= \frac{4(1-c_2)(1-c_3)}{3c_1^2}G_h + \frac{(1-c_3)(1-c_{2\theta})}{c_1 c_{1\theta}}G_h \\
\chi_3 &= \frac{2(1-c_2)}{3c_1 c_{1\theta}}G_m \\
\chi_4 &= 1 - \frac{4(1-c_3)}{3c_1 c_{1\theta}}G_h - \frac{c_{\epsilon\theta}(1-c_{3\theta})}{c_{1\theta}}G_h \\
\chi_5 &= \frac{2(1-c_2)}{3c_1} \\
\chi_6 &= \frac{2}{3c_{1\theta}}.
\end{aligned}$$

Linkage of c_m and c_h to the mean fields is thus provided through non-dimensional vertical gradients G_m and G_h, defined, respectively, as

$$G_m = \frac{E^2}{\epsilon^2}\left[\left(\frac{\partial U}{\partial z}\right)^2 + \left(\frac{\partial V}{\partial z}\right)^2\right], \tag{A3}$$

$$G_h = -\frac{E^2}{\epsilon^2}\frac{g}{\Theta_a}\frac{\partial \Theta}{\partial z}. \tag{A4}$$

The gradient Richardson number, $\mathrm{Ri} = -G_h/G_m$, can be written in terms of these. From Section 2.1, this is related to the flux Richardson number through

$$\mathrm{Ri}_f = \frac{c_h}{c_m}\mathrm{Ri}. \tag{A5}$$

Closure parameters c_1, $c_{1\theta}$, c_2, $c_{2\theta}$, c_3, $c_{3\theta}$ and $c_{\epsilon\theta}$ arrive from models for pressure redistribution and potential temperature variance dissipation terms in the GL78 SOC. We maintain the GL78 values $[c_1, c_{1\theta}, c_2, c_{2\theta}, c_3, c_{3\theta}] = [1.8, 3.0, 0.6, 0.33, 0.5, 0.33]$.

A special case of the Level-2.5 model (termed Level-2 in Mellor and Yamada's terminology) is that for local equilibrium, in which (7) reduces to (10). Inserting (4) and (5) into (8), substituting into (10) and rearranging leads to $G_{m,LE} = 1/(c_{m,LE}(1-\mathrm{Ri}_{f,LE}))$ and $G_{h,LE} = -\mathrm{Ri}_{f,LE}/(c_{h,LE}(1-\mathrm{Ri}_{f,LE}))$, where $G_{m,LE}$, $G_{h,LE}$, $c_{m,LE}$, $c_{h,LE}$ and $\mathrm{Ri}_{f,LE}$ are the local equilibrium forms of these variables. Substituting these for G_m and G_h into the χ_i functions in (A1) and (A2) then leads after algebra to

$$c_{m,LE} = c_{m,0}\left[\frac{(1-\Gamma_1\mathrm{Ri}_{f,LE})(1-\Gamma_2\mathrm{Ri}_{f,LE})}{(1-\mathrm{Ri}_{f,LE})(1-\Gamma_3\mathrm{Ri}_{f,LE})}\right] \tag{A6}$$

$$c_{h,LE} = c_{h,0}\left(\frac{1-\Gamma_1\mathrm{Ri}_{f,LE}}{1-\mathrm{Ri}_{f,LE}}\right), \tag{A7}$$

where

$$\begin{aligned}
c_{m,0} &= \frac{2(1-c_2)(c_1+c_2-1)}{3c_1^2} \\
c_{h,0} &= \left[\frac{c_1}{c_{1\theta}(1-c_2)}\right]c_{m,0} \\
\Gamma_1 &= \frac{c_1 + 2(1-c_3) + 1.5c_1c_{\epsilon\theta}(1-c_{3\theta})}{c_1+c_2-1} \\
\Gamma_2 &= \frac{c_1+2(1-c_3)}{c_1+c_2-1} + \frac{1.5c_1(1-c_3)(1-c_{2\theta})}{c_{1\theta}(1-c_2)(c_1+c_2-1)} \\
\Gamma_3 &= \Gamma_1 - 1.5\left(\frac{1-c_3}{c_1+c_2-1}\right).
\end{aligned}$$

Substituting (A6) and (A7) for c_m and c_h, respectively, into (A5), setting $\mathrm{Ri}_f = \mathrm{Ri}_{f,LE}$ on the left side, and solving the resulting quadratic then gives

$$\mathrm{Ri}_{f,LE} = \frac{1}{2\Gamma_2}\left(1 + \Gamma_5 \mathrm{Ri} - \sqrt{1 + 2(\Gamma_5 - 2\Gamma_4)Ri + \Gamma_5^2 \mathrm{Ri}^2}\right), \tag{A8}$$

where $\Gamma_4 = \Gamma_2/Pr_{t,0}$, $\Gamma_5 = \Gamma_3/\mathrm{Pr}_{t,0}$ and $\mathrm{Pr}_{t,0} = c_{m,0}/c_{h,0}$. The two independent variables (G_m and G_h) in (A1) and (A2) therefore reduce to one (Ri) in (A6) and (A7), i.e., when local equilibrium is assumed. Using the above closure parameter values, it can be shown that $\Gamma_1 > \Gamma_2$ and $\Gamma_1 > \Gamma_3$. As such, it is seen from (A6) and (A7) that $Ri_{f,c} = 1/\Gamma_1$ defines a 'critical' value at which $c_{m,LE}$ and $c_{h,LE}$ are zero. The domain of (A6)-(A8) is thus $0 \leq \mathrm{Ri}_{f,LE} \leq \mathrm{Ri}_{f,c}$, with the above closure parameter values giving $\mathrm{Ri}_{f,c} = 0.247$.

Appendix B: Analysis of the TKE Transport Term

In steady-state, (7) can be rearranged and expressed symbolically as

$$0 = P_{\mathrm{tot}}\left(1 + \frac{T_E}{P_{\mathrm{tot}}}\right) - \epsilon, \tag{B1}$$

where $P_{\mathrm{tot}} = P(1 - \mathrm{Ri}_f)$ and $T_E = d/\mathrm{d}z(\sigma_E^{-1} K_m \,\mathrm{d}E/\mathrm{d}z)$. The local equilibrium assumption, $P_{\mathrm{tot}} = \epsilon$, therefore requires $T_E/P_{\mathrm{tot}} << 1$.

Letting $P_{\mathrm{tot}} = \epsilon$ and applying to T_E the enumerated procedure leading to (29), the following *a posteriori* approximation of T_E/P_{tot} is obtained,

$$\frac{T_E}{P_{\mathrm{tot}}} \approx \left(\frac{k^2}{\sigma_E}\right)\frac{\mathrm{Ri}_f(1 - \beta \mathrm{Ri}_f)^2}{(1 - \mathrm{Ri}_f)}\left[(1 - 3\beta \mathrm{Ri}_f)(1 - \beta \mathrm{Ri}_f)\frac{\mathrm{d}\tilde{E}}{\mathrm{dRi}_f}\right.$$

$$\left. + \mathrm{Ri}_f(1 - \beta \mathrm{Ri}_f)^2 \frac{\mathrm{d}^2\tilde{E}}{\mathrm{dRi}_f{}^2}\right], \tag{B2}$$

where $\tilde{E} = c_{m,LE}^{-1/2}(1 - \mathrm{Ri}_f)^{1/2}$. A plot of (B2) for $0 \leq \mathrm{Ri}_f \leq 1/\beta$ ($\beta = 4.7$) is shown in Figure B1. Here, $\tilde{E}$ is computed using (A6) for $c_{m,LE}$. Although the first and second derivatives of $\tilde{E}$ appearing in (B2) can be worked out analytically, we instead for simplicity computed these numerically using a node spacing $\Delta \mathrm{Ri}_f = 0.001$; doubling and halving this yielded results that are graphically indistinguishable from those in the figure.

It is seen that $T_E/P_{\mathrm{tot}} \approx \mathrm{O}(10^{-3})$ over the entire Ri_f range, sufficiently small to justify the local equilibrium assumption on (7).

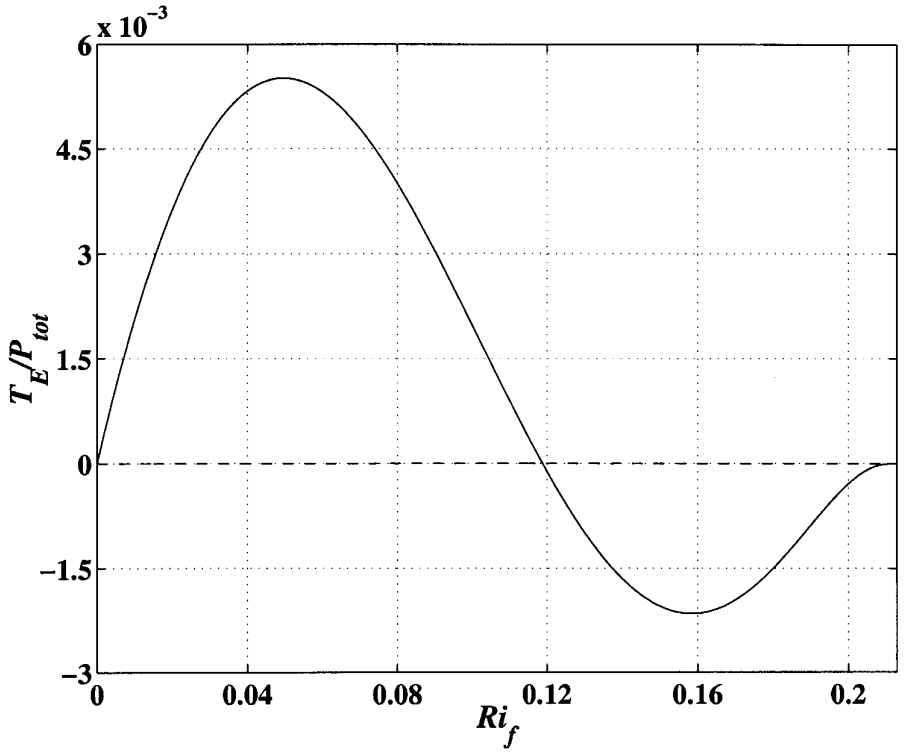

Figure B1. Ratio of TKE transport to total production term as a function of Ri_f, as computed from (B2). See Appendix B for details.

References

André, J. C. and Mahrt, L.: 1982, 'The Nocturnal Surface Inversion and Influence of Clear-Air Radiative Cooling', *J. Atmos. Sci.* **39**, 864–878.

Andrén, A.: 1990, 'Evaluation of a Turbulence Closure Scheme Suitable for Air Pollution Applications', *J. Appl. Math. Phys.* **29**, 224–239.

Andrén, A.: 1991, 'A TKE-Dissipation Model for the Atmospheric Boundary Layer', *Boundary-Layer Meteorol.* **56**, 207–221.

Apsley, D. D. and Castro, I. P.: 1997, 'A Limited-Length-Scale $k - \epsilon$ Model for the Neutral and Stably-Stratified Atmospheric Boundary Layer', *Boundary-Layer Meteorol.* **83**, 75–98.

Arya, S. P. S.: 1975, 'Geostrophic Drag and Heat Transfer Relations for the Atmospheric Boundary Layer', *Quart. J. Roy. Meteorol. Soc.* **101**, 147–161.

Baumert, H. and Peters, H.: 2000, 'Second-Moment Closures and Length Scales for Weakly Stratified Turbulent Shear Flows', *J. Geophys. Es. – Oceans* **105**, 6453–6468.

Brost, R. A. and Wyngaard, J. C.: 1978, 'A Model Study of the Stably-Stratified Planetary Boundary Layer', *J. Atmos. Sci.* **35**, 1427–1440.

Brown, A. R., Derbyshire, S. H., and Mason, P. J.: 'Large-Eddy Simulation of Stable Atmospheric Boundary Layers with a Revised Stochastic Subgrid Model', *Quart. J. Roy. Meteorol. Soc.* **120**, 1485–1512.

Businger, J. A., Wyngaard, J. C., Izumi, Y., and Bradley, E. F.: 1971, 'Flux-Profile Relationships in the Atmospheric Surface Layer', *J. Atmos. Sci.* **28**, 181–189.

Caughey, S. J. Wyngaard, J. C., and Kaimal, J. C.: 1979, 'Turbulence in the Evolving Stable Boundary Layer', *J. Atmos. Sci.* **36**, 1041–1052.

Coleman, G., Ferziger, J., and Spalart, P.: 1992, 'Direct Simulation of the Stably Stratified Turbulent Ekman Layer', *J. Fluid Mech.* **244**, 677.

Delage, Y.: 1997, 'Parameterising Sub-Grid Scale Vertical Transport in Atmospheric Models under Statically Stable Conditions', *Boundary-Layer Meteorol.* **82**, 23–48.

Derbyshire, S. H.: 1990, 'Nieuwstadt's Stable Boundary Layer Revisited', *Quart J. Roy. Meteorol. Soc.* **116**, 127–158.

Derbyshire, S. H.: 1995, 'Stable Boundary Layers: Observations, Models and Variability Part I: Modelling and Measurements', *Boundary-Layer Meteorol.* **74**, 19–54.

Durbin, P. A. and Pettersson-Reif, B. A.: 2001, *Statistical Theory and Modeling for Turbulent Flow*, John Wiley and Sons, Chichester, U.K., 282 pp.

Duynkerke, P. G.: 1988, 'Application of the $E - \epsilon$ Turbulence Closure Model to the Neutral and Stable Atmospheric Boundary Layer', *J. Atmos. Sci.* **45**, 865–880.

Freedman, F. R. and Jacobson, M. Z.: 2002, 'Transport-Dissipation Analytical Solutions to the $E - \epsilon$ Turbulence Model and their Role in Predictions of the Neutral ABL', *Boundary-Layer Meteorol.* **102**, 117–138.

Garratt, J. R.: 1992, *The Atmospheric Boundary Layer*, University Press, Cambridge, 316 pp.

Grant, A. L. M.: 1997, 'An Observational Study of the Evening Transition Boundary Layer', *Quart. J. Roy. Meteorol. Soc.* **123**, 657–677.

Högström, U.: 1988, 'Non-Dimensional Wind and Temperature Profiles in Atmospheric Surface-Layer: A Reevaluation', *Boundary-Layer Meteorol.* **42**, 55–78.

Howell, J. F. and Sun, J.: 1999, 'Surface-Layer Fluxes in Stable Conditions', *Boundary-Layer Meteorol.* **90**, 495–520.

Kosovic, B. and Curry, J. A.: 2000, 'A Large Eddy Simulation of a Quasi-Steady, Stably Stratified Atmospheric Boundary Layer', *J. Atmos. Sci.* **57**, 1052–1068.

Lacser, A. and Arya, S. P. S.: 1986, 'A Comparative Assessment of Mixing-Length Parameterizations in the Stably Stratified Nocturnal Boundary Layer (NBL)', *Boundary-Layer Meteorol*. **36**, 53–70.

Launder, B. E.: 1989, 'Second-Moment Closure ... and Future?', *Int. J. Heat Fluid Flow* **10**, 282–300.

Lenschow, D. H., Li, X. S., Zhu, C. J., and Stankov, B. B.: 1998, 'The Stably Stratified Boundary-Layer over the Great Plains: 1. Mean and Turbulence Structure', *Boundary-Layer Meteorol.* **42**, 95–121.

Mahrt, L.: 1999, 'Stratified Atmospheric Boundary Layers', *Boundary-Layer Meteorol.* **90**, 375–396.

Mellor, G. L. and Yamada, T.: 1982, 'Development of a Turbulence Closure Model for Geophysical Fluid Problems', *Rev. Geophys. Space Phys.* **20**, 851–875.

Nieuwstadt, F. T. M.: 1984, 'The Turbulent Structure of Stable, Nocturnal Boundary Layer', *J. Atmos. Sci.* **41**, 2202–2216.

Nieuwstadt, F. T. M.: 1985, 'A Model for Stationary, Stable Boundary Layer', in J. C. R. Hunt (ed.), *Turbulence and Diffusion in Stable Environments*, Clarendon Press, pp. 149-179.

Ohya, Y.: 2001, 'Wind-Tunnel Study of Atmospheric Stable Boundary Layers over a Rough Surface', *Boundary-Layer Meteorol.* **98**, 57–82.

Sorbjan, Z.: 1989, *Structure of the Atmospheric Boundary Layer*, Prentice Hall, Englewood, 317 pp.

Speziale, C. G. and Bernard, P. S.: 1992, 'The Energy Decay of Self-Preserving Isotropic Turbulence Revisited', *J. Fluid Mech.* **241**, 645–667.

Speziale, C. G. and Gatski, T. B.: 1996, 'Analysis and Modelling of Anisotropies in the Dissipation Rate of Turbulence', *J. Fluid Mech.* **344**, 155–180.

Speziale, C. G. and MacGiolla-Mhuiris, N.: 1989, 'On the Prediction of Equilibrium States in Homogeneous Turbulence', *J. Fluid Mech.* **209**, 591–615.

Tennekes, H. and Lumley, J. L.: 1972, *A First Course on Turbulence*, MIT Press, Cambridge, MA, 300 pp.
Wilcox, D. C.: 1998, *Turbulence Modeling for CFD*, DCW Industries Inc., La Canada, CA.
Wyngaard, J. C.: 1975, 'Modeling the Planetary Boundary Layer - Extension to the Stable Case', *Boundary-Layer Meteorol.* **71**, 277–296.